DIELECTRIC DISCHARGE CHARACTERISTICS IN A TWO-ELECTRON SIMULATION ENVIRONMENT*

**M. Treadaway, R. Leadon, C. Mallon,
T. Flanagan, R. Denson, and E. Wenaas
JAYCOR**

INTRODUCTION

In the space environment, electrons are present with energies from a few eV to several MeV. Most studies of the charging of spacecraft dielectrics have focused on charging by the low-energy (5 to 20 keV) portion of the space electron spectrum. As part of the Air Force Weapons Laboratory (AFWL)-sponsored electron-caused electromagnetic pulse (ECEMP) program, the effect of the high-energy portion of the electron spectrum on the charging of spacecraft dielectrics was investigated. Results of an initial series of experiments performed at accelerated fluxes indicated that the charging and discharging characteristics of spacecraft dielectrics are significantly altered by the presence of high-energy electrons (refs. 1,2,3). In this paper, the results of a second series of experiments, in which flux levels more representative of the space electron environment were used, are presented and compared to the results of the high flux tests. The simulation approach was to partition the space electron spectrum into two parts, those electrons which do not penetrate a material and therefore contribute to charging and those which completely penetrate the material. The non-penetrating electrons were simulated using 25-keV electrons and the penetrating electrons by 350-keV electrons.

The materials included in this investigation were Kapton, optical solar reflectors (OSRs), and a ground test satellite surface potential monitor which contained Kapton, Astroquartz, OSRs and Teflon.

EXPERIMENTAL DETAILS

The low flux experiments were performed in the AFWL 4-m-diameter, 6-m-long vacuum chamber shown in figure 1. During these tests, the chamber pressure was maintained between 5 and 8 x 10^{-6} torr. A Kimball Physics electron flood gun was used as a source of 6 to 25 keV electrons and a High Voltage Engineering Van de Graaff as a source of 350 to 450 keV electrons. Both electron beams were collimated and rastered. The current densities of the low energy (6 to 25 keV) and high energy (350 to 400 keV) electrons could be varied from 5 to 350 pA/cm^2 and 1.0 to 60 pA/cm^2, respectively (measured at the sample location). Current densities were measured using 195 cm^2 aluminum stopping blocks which were connected to a current meter.

*Work sponsored by AFWL under Computer Sciences Corporation Subcontract S-220.

The test samples included a 400 cm^2 array of twenty 8 mil OSRs, a 25 cm diameter sample of 2 mil aluminized Kapton, and four samples (3 mil Teflon, 5 mil aluminized Kapton, 8 mil OSRs and Astroquartz) mounted in a ground test version of the SCATHA Satellite Surface Potential Monitor (SSPM).

The 8 mil OSRs and 2 mil Kapton samples were placed on aluminum mounting plates. The mounting plates were each connected to ground through a one-ohm resistor across which discharge-induced voltages were measured with an oscilloscope. The samples were mounted in a sample carousel and a shielding plate in front of the carousel could be removed remotely to allow irradiation of the samples. Measurements of the surface potential of these samples were performed using a scanning capacitive divider electrostatic voltmeter (ESV). The ESV was fabricated by JAYCOR and was calibrated prior to and during the experimental sequence by biasing the sample mounting plates to potentials from -1 to -10 kV.

The SSPM was mounted directly above the sample carousel. The SSPM electronics were used to monitor the surface potential and leakage currents of the SSPM samples.

ENVIRONMENT AND SIMULATION

Figure 2 shows two electron spectra measured at geosynchronous altitudes. As a first approximation for simulation, these spectra were partitioned into non-penetrating and penetrating electrons. The non-penetrating electrons were simulated using a monoenergetic low energy electron beam (6 to 25 keV) and the penetrating electrons were simulated using a monoenergetic high energy electron beam (350 to 400 keV)*. Using this simulation philosophy the spectra shown in figure 2 would be simulated by the fluxes listed in table 1. These fluxes were determined from consideration of the practical range of electrons in the test materials which is material dependent. Also listed in table 1 are the ranges of fluxes available during the tests described in this paper.

For a planar sample in a steady-state charging condition, charge conservation requires that

$$J_B - J_S - J_L - J_P = 0 \qquad (1)$$

where J_B is the current density of electrons that stop in the sample, J_S is the secondary electron emission current density, J_L is the leakage current density and J_P is the photoemission current density.

*The practical range of a 350 keV electron in SiO_2 is roughly 0.053 cm (≈21 mils) and the thickest sample tested was the 8 mil OSRs.

The secondary electron current is a function, δ, of the energy, E_B, of the electron beam, the incident electron current density, and the sample surface potential, V. J_S can be written as

$$J_S = J_B \, \delta(E_B - V) \tag{2}$$

If the penetration depth of the incident low energy electrons is small compared to the thickness, L, of the dielectric sample and if the conductivity, σ, of the dielectric is uniform, then the leakage current density can be written as

$$J_L = \frac{V}{L} \sigma$$

The conductivity of the bulk dielectric is the sum of the ambient and radiation-enhanced conductivities, σ_A and σ_R, respectively. The radiation induced conductivity can be written as

$$\sigma_{rad} = K\dot{\gamma}^{\Delta} = K \cdot J_{Pen}^{\Delta}$$

where K and K are material dependent constants, $\dot{\gamma}$ is the radiation dose rate of the penetrating electrons, J_{Pen} is the current density of penetrating electrons and Δ is a material dependent constant which has values between 0.8 to 1.0 for most materials. Thus, the total conductivity can be written as

$$\sigma = \sigma_A + K\dot{\gamma}^{\Delta} \tag{4}$$

If the sample is in the dark, the photoemission current can be considered to be negligible.

Manipulation of equations (1), (2), and (3) yields the surface potential as a function of the incident electron current density in the form

$$V = \frac{J_B L}{\sigma} [1 - \delta(E_B - V)] \tag{5}$$

For exposure to non-penetrating electrons only, at beam energies significantly larger than the secondary electron second crossover energy, V_S, the function δ in equation (5), will be small compared to unity and the potential will increase linearly from zero as a function of J_B/σ. At larger values of the surface potential, δ will no longer be negligible and the potential will asympototically approach a value V_m given by

$$V_m = E_B - V_S \tag{6}$$

assuming that the dielectric does not break down first. Obviously from equation (6) the asymptotic value of the surface potential is different for different beam energies. Figure 3 shows plots of V versus J_B/σ for 2 mil and 5 mil (L = 0.005 and 0.0127 cm, respectively) samples, where a value for V_S of 1.5 kV has been assumed, which is approximately the value for the secondary emission crossover of Kapton. The shape of the transition region from the linearly increasing curve to the horizontal asymptote was estimated using the secondary emission curve for Kapton given in reference 6.

If a Kapton sample is simultaneously exposed to non-penetrating, e.g., 10 keV, and totally penetrating electrons, then several limiting cases can be considered. If the flux of penetrating electrons is small such that the rate of energy deposition due to the penetrating electrons produces only a negligible increase in the conductivity of the Kapton, then the surface potential will be dominated by the ambient conductivity and can achieve a maximum value of ≈8.5 kV. If, however, the flux of penetrating electrons is sufficiently large so as to increase the conductivity well above the ambient conductivity, i.e., $\sigma_R \gg \sigma_A$, , then the surface potential will be given by

$$V = \frac{J_B L}{K' J_P^{\Delta}} [1 - \delta(E_B - V)] \tag{7}$$

As can be seen in Figure 3, the equilibrium surface potential will be less than 8.5 kV as the conductivity increases, assuming the flux of non-penetrating electrons remains the same. Thus, it can be seen that the effect of the penetrating electrons on the equilibrium surface potential is a function of the flux of non-penetrating electrons and penetrating electrons as well as the secondary electron emission properties, the ambient conductivity and the radiation-induced conductivity coefficient of the exposed material.

Equation (7) predicts that for some conditions the potential to which a material will charge upon exposure to non-penetrating and penetrating electrons will be independent of the absolute magnitudes of the electron current densities and will be dependent only on the ratio of the fluxes of the non-penetrating and penetrating electrons.

EXPERIMENTAL RESULTS

OSR's

When the OSRs were exposed to low energy (25 keV) electrons alone, discharge currents on the order of 28 to 35 A were measured. Table 2 lists a comparison of the discharge characteristics data obtained during the low flux tests and the previously reported high flux tests (refs. 1,2). In general, one can conclude that there is at most only a small dependence of the discharge characteristics upon the exposure flux in the range of 0.19 to 5 nA/cm^2.

When the OSRs were exposed to high- and low-energy electrons simultaneously, discharges occurred only when the ratio of the low- to high-energy electron flux was greater than 63 to 76. Figure 4 shows a comparison of the discharge pulses observed for low energy electron exposure and combined low- and high-energy electron exposure. Note that the peak discharge current observed during the combined energy electron exposure is only 1.3 A which is roughly 1/25 the peak current observed during the low-energy electron exposures. When the ratio of the low energy and high energy electron fluxes was less than 63 to 76 no discharges were observed and measurements of the equilibrium surface potential after these exposures showed the surface potential to be less than 5 kV.

Table 3 shows a comparison of OSR discharge characteristics obtained during the low and high flux tests. The results are effectively the same with the exception of the discharge threshold data, which indicates that the discharge threshold in the combined energy electron exposures was lower in the high flux test than in the low flux tests. Since the high flux tests (refs. 1,2) were originally performed in a different facility than the low flux tests, a series of additional high flux tests were performed in the low flux test chamber to discriminate between actual flux effects and possible facility effects. This second series of high flux tests indicated a threshold potential for discharge for the OSRs of 5 to 6 kV which is in agreement with the low flux test results. No explanation for the relatively low discharge threshold potential determined in the original high flux tests has been proposed at this time.

KAPTON

When the 2 mil Kapton sample was exposed to low energy (25 keV) electrons alone at fluxes greater than 1 or 2 nA/cm^2, the sample charged up to 13 kV at which time discharges occurred (Ref. 1). When the sample was exposed to a combined high- and low-energy electron environment, no discharges occurred and the surface potential remained well below the 13 kV discharge threshold. Figure 5 shows the Kapton surface potential measured after exposure of the sample to combined high- and low-energy electron environments with various relative fluxes. The relative fluxes are given as the ratio of the low energy electron current density to the dose rate of the high energy electrons [where a conversion factor of 560 $(rad/s)/(nA/cm^2)$ has been used]. The data labeled Phase II was obtained in the high flux tests which were performed at rates roughly 5 to 100 times those for which the low flux (Phase III) data was obtained. The data indicates a linear dependence of the surface potential on the ratio of the low to high energy electron fluxes. This linear dependence is predicted by equation (7) when $\delta(E_B - V)$ is either small or a constant. Equation (7), however, predicts a zero intercept for the surface potential, whereas the data indicates an intercept of roughly 1.1 kV. It is interesting to note that for a two-energy simulation of the electron distributions shown in figure 2, the ratio of the non-penetrating to the penetrating electron fluxes can be determined from table 1 to be 2×10^{-3} and 0.57 $(rad/s)/(nA/cm^2)$ for the "AE4" and "SCATHA" environments, respectively. From figure 5 this would imply that the 2-mil Kapton would charge to 1.1 and 8.1 kV respectively in these environments.

From the data shown in figure 5 and the curves shown in figure 3, values for the radiation-induced conductivity coefficient, K, can be determined. In figure 5, an equilibrium surface potential of 2 kV is associated with a flux ratio of 0.07 $(nA/cm^2)/(rad/s)$. From figure 3 an equilibrium surface potential of 2 kV is associated with a value of J_B/σ of 0.37×10^6 V/cm. Since

$$\frac{J_B}{\sigma} = \frac{J_B}{\dot{\gamma}K}$$

if $V_B \gg V_S$ and $\sigma_{rad} \gg \sigma_A$ then a value of the radiation-induced conductivity coefficient can be determined by

$$K = \left(\frac{J_B}{\dot{\gamma}}\right) \cdot \left(\frac{\sigma}{J_B}\right) = 1.9 \times 10^{-16} \text{ (ohm-cm)/(rad/s)}$$

This value is roughly an order of magnitude or more larger than published values (ref. 7). It is important to note, however, that the method of measuring radiaton-induced conductivities often involves placing a bias across a dielectric by means of electrodes and measuring the currents that flow upon either pulsed or continuous radiation exposures. It is conceivable that the conductivity measured by this technique, while applicable to many radiation problems, results in a lower value of the radiation-induced conductivity than would be measured by monitoring the conduction of embedded electrons.

SSPM

Upon exposure to low energy (6 to 10 keV) electrons alone, the SSPM 5 mil Kapton sample charged to potentials roughly equal to the beam energy minus the secondary emission second cross over potential. When the SSPM was exposed to a combined low (10 keV) and high (450 keV) energy electron environments the equilibrium surface potential was only about 1000 volts less than that observed during the low energy electron exposures as shown in table 4. This result was surprising in light of the results presented above. Using the value for K of 1.6×10^{-16} ohm/cm/(rad-s) determined above, the radiation-induced conductivity during the combined energy electron exposures would have been on the order of 5.6×10^{-16} ohm-cm. Thus, for the combined 10 keV and 450 keV electron exposure

$$\frac{J_B}{\sigma} = \frac{200 \times 10^{-12}}{5.6 \times 10^{-16}} = 3.4 \times 10^5 \text{ V/cm}$$

Referring to figure 3 for a 5-mil Kapton sample, one would expect the equilibrium surface potential to be on the order of 3.8 kV as opposed to the 6.99 kV that was measured by the SSPM.

In subsequent tests the SSPM Kapton sample was charged to roughly 8 kV using only a 10 keV electron beam. The 10 keV beam was turned off and the surface potential of the sample was monitored while the sample was exposed to 350 keV electrons only. Figure 6 shows the surface potential measured during

this experiment as a function of exposure time. When the 350 keV electron beam current was increased from 1 to 5 pA/cm^2, the decay of the surface potential did not accelerate and thus the decay of the surface potential is apparently due primarily to the basic conductivity of the sample. Measurements of the leakage current through the sample via the SSPM instrumentation, however, indicated as much as a factor of 40 increase in the leakage current when high energy electrons were incident on the sample as compared to the leakage current measured when only low energy electrons were incident on the sample. This observation indicates that the conductivity of the SSPM 5 mil Kapton sample is greatly enhanced by the presence of the high energy electrons. These apparently contradictory results led us to question the method by which the SSPM measures surface potential. As shown in figure 7 the SSPM measures surface potential at the rear of the sample at a point from which the vacuum deposited aluminum has been removed. The diameter of the hole in the metalization is large compared to the thickness of the material (diameter/thickness ≈20). The 6 to 25 keV electrons which stop near the surface of the material in the center of the hole and subsequently flow to the nearest ground plane must move a much larger distance than those trapped in the Kapton over areas where the metalization is intact. Thus, in the region of the hole the effective thickness of the material for conductivity calculations is larger than the thickness of the material. The ratio of the average distance that the trapped electrons must travel in the hole region to reach the ground plane (~0.5 x hole radius) to the sample thickness is about 10. If one ratioed the predicted 3800 volts for a fully metalized 5-mil sample by this factor, to determine the potential in the hole region, the potential would be greater than the beam voltage. Thus, it would not be unexpected that the potential as measured in the hole region would be larger than that predicted for a fully metalizer 5-mil sample and would approach the measured SSPM surface potential for low-energy electron exposure (8250 volts).

The data for the other SSPM samples has not been reduced at this time.

CONCLUSIONS

From a comparison of the low and high flux data as well as comparison of the data from low energy monoenergetic electron exposures and combined low and high energy electron exposures, one can conclude:

1. The presence of high energy electrons can significantly affect the charging and discharging characteristics of spacecraft dielectrics,

2. Discharge currents in combined-energy electron simulation environments can be considerably lower than those in low energy electron simulation environments,

3. Equilibrium surface potentials will often be held below discharge threshold potentials due to enhanced conductivity caused by the high energy electrons,

4. Over a wide range of simulation current densities, accelerated rate testing appears not to affect the test results as long as the ratio

of low energy to high energy electron fluxes is preserved, and

5. In space environments where high energy electrons are present, the surface potential at the SSPM measurement area may be higher than the surface potential over the remainder of the SSPM sample area.

The primary implication of these conclusions is that charging and discharging characterization data obtained from low energy electron simulations of space environments will lead one to expect much larger discharge currents and more frequent discharges than may occur in space environments.

REFERENCES

1. Treadaway, M. J., et al.: The Effects of High Energy Electrons on the Charging of Spacecraft Dielectrics. IEEE Trans. Nucl. Sci., NS-26, no. 6, Dec. 1979.

2. Treadaway, M. J., et al.: Effects of Laboratory Simulation Parameters on Spacecraft Dielectric Discharges. JAYCOR report no. 200-79-155, July 1979.

3. Treadaway, M. J., et al.: ECEMP Phase III Low Flux Tests. JAYCOR report no. 200-80-235/2176, July 1980.

4. Panlikas, G. A.: Electron Irradiation in Synchronous Orbit. Aerospace Tech. Memo 7616260-201-3, Aug. 3, 1976.

5. Mizera, Paul, Aerospace Corp., March 1980, private communication.

6. Katz, I., et al.: A Three Dimensional Dynamic Study of Electrostatic Charging in Materials. NASA CR-135356, Aug. 1977.

7. Ahrens, T. F., and Wooten, F.: Electrical Conductivity Induced in Insulators by Pulsed Radiation. IEEE Trans. Nucl. Sci., NS-12, June 1976.

TABLE 1. ENVIRONMENTAL SIMULATION FLUXES

MATERIAL	AE4 ENVIRONMENT 25 keV (pA/cm^2)	AE4 ENVIRONMENT 350 keV (pA/cm^2)	SCATHA ENVIRONMENT 25 keV (pA/cm^2)	SCATHA ENVIRONMENT 350 keV (pA/cm^2)
KAPTON (2 mil)	7.4	6.2	96	0.3
KAPTON (5 mil)	9.6	3.2	96	0.2
OSR ARRAY	10	1.7	96	0.05

FLUX RANGES ACHIEVABLE

25 keV: $5 < J < 350\ pA/cm^2$
350 keV: $1 < J < 60\ pA/cm^2$

TABLE 2. COMPARISON OF OSR DISCHARGE CHARACTERISTICS IN 25 keV ELECTRON ENVIRONMENT AT LOW AND HIGH FLUXES

	PHASE III RESULTS	PHASE II RESULTS
DISCHARGE THRESHOLD (kV)	5-6	~ 2
RETURN CHARGE (μC)	0.2 (25 keV, 0.29 nA/cm^2) (350 keV, 0.003 nA/cm^2)	0.5-1.0 (25 keV, 13 nA/cm^2) 350(keV, 0.17 nA/cm^2)
FLUX AT WHICH DISCHARGES BEGIN(J_{low}/J_{high})	~ 63	~ 76

TABLE 3. COMPARISON OF OSR DISCHARGE CHARACTERISTICS IN COMBINED ENERGY ELECTRON ENVIRONMENTS AT LOW AND HIGH FLUXES

	PHASE III (0.19 nA/cm^2)	PHASES I AND II (1-5 nA/cm^2)
DISCHARGE THRESHOLD (kV)	6.5-7.5	6-7
PEAK CURRENT (amps)	28	35
RETURN CHARGE (μC)	16	28-24
PULSE WIDTH, Q/I_p (μsec)	0.57	0.68 - 0.8
FREQUENCY OF DISCHARGE (#/min)	0.08	0.1[a]

[a] EXTRAPOLATED LINEARLY TO 0.19 nA/cm^2

TABLE 4. SSPM KAPTON SURFACE POTENTIAL VS EXPOSURE CONDITIONS

LOW ENERGY ELECTRON BEAM ENERGY (Flux)	EQUILIBRIUM SURFACE POTENTIAL (kV)		
	LOW ENERGY ELECTRONS ONLY (Measured)	COMBINED ENVIRONMENT (450 keV, 5 pA/cm^2)	
		MEASURED BY SSPM	PREDICTED
6 keV(200pA/cm^2)	3350	---	---
8 keV(200pA/cm^2)	6430	5450	---
10 keV(200pA/cm^2)	8250	> 6990	3800

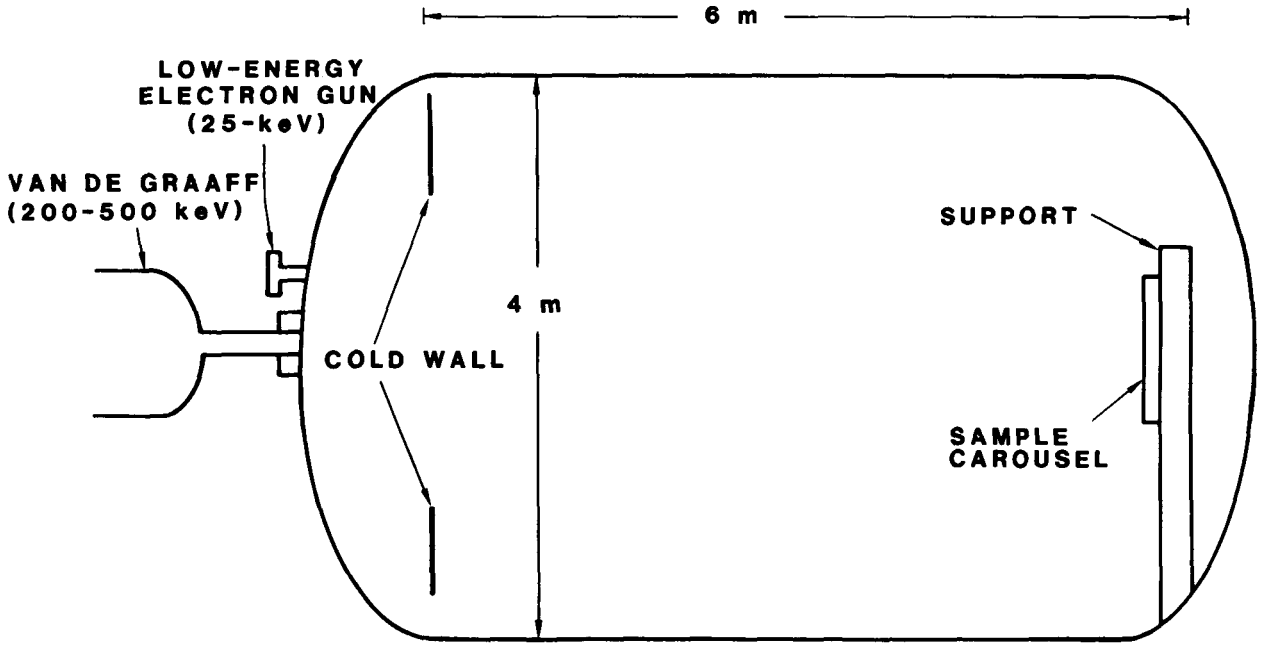

FIGURE 1. OVERVIEW OF THE LOW FLUX TEST FACILITY

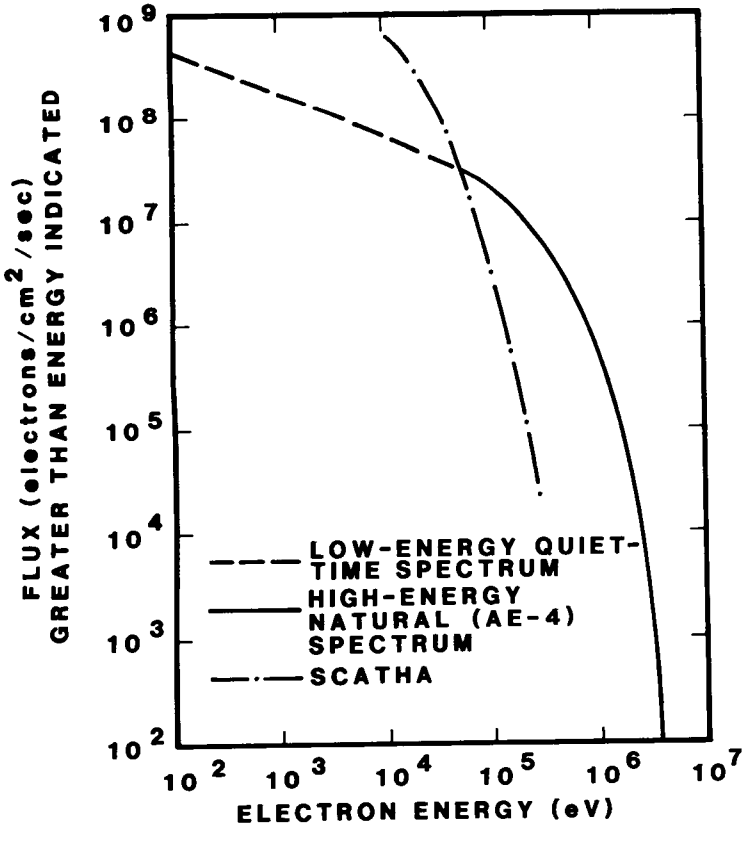

FIGURE 2. TWO ELECTRON ENERGY DISTRIBUTIONS AT SYNCHRONOUS ALTITUDE

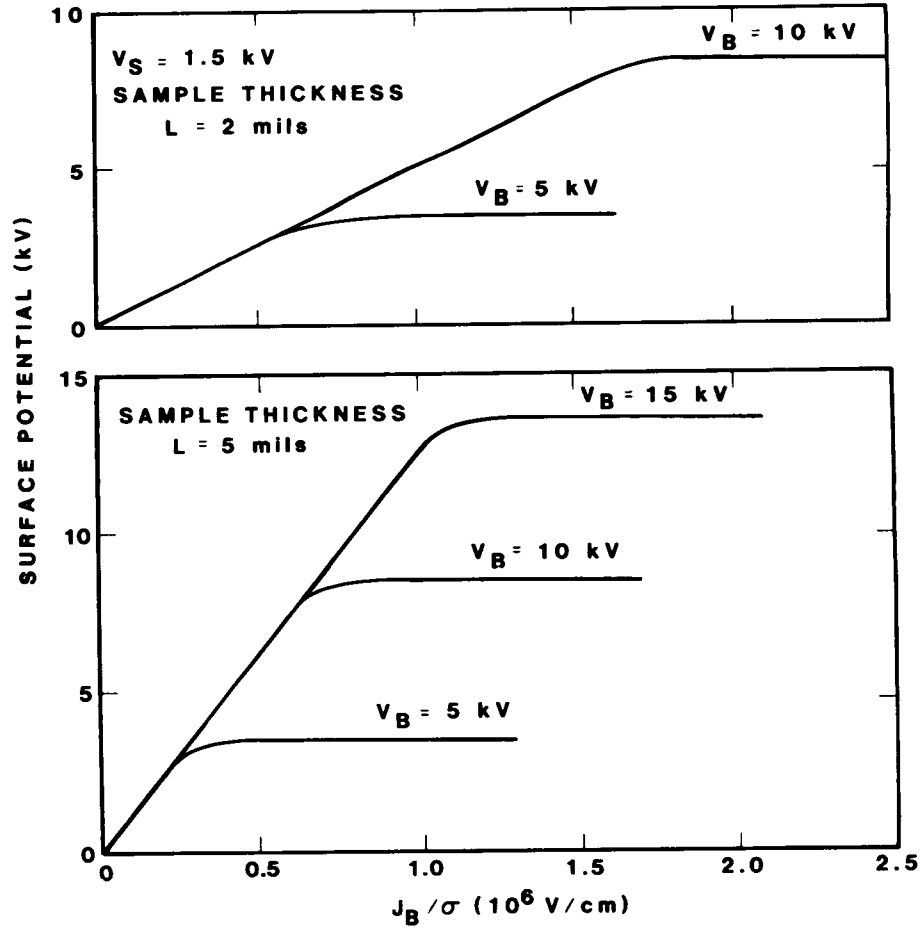

FIGURE 3. VARIATION OF SURFACE POTENTIAL, V, WITH LOW-ENERGY BEAM CURRENT, J_B, AND BULK CONDUCTIVITY, σ

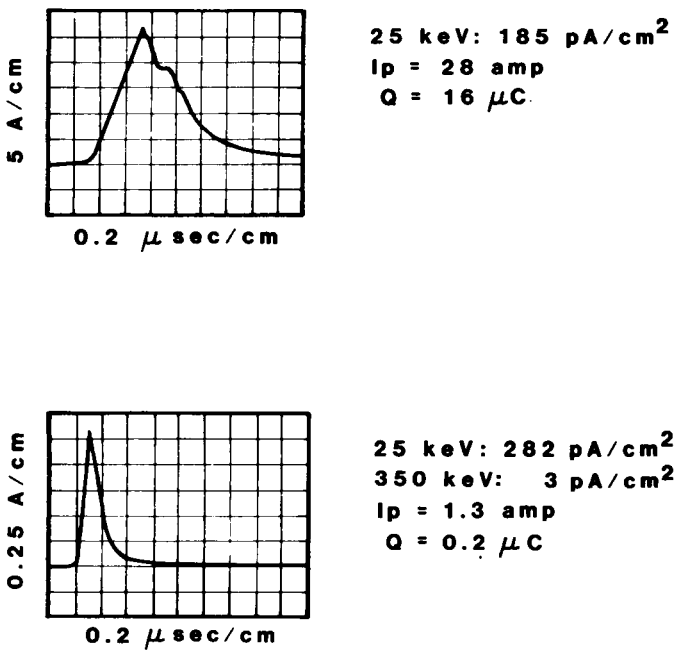

FIGURE 4. COMPARISON OF OSR DISCHARGES IN LOW ENERGY AND COMBINED LOW AND HIGH ENERGY ELECTRON ENVIRONMENTS

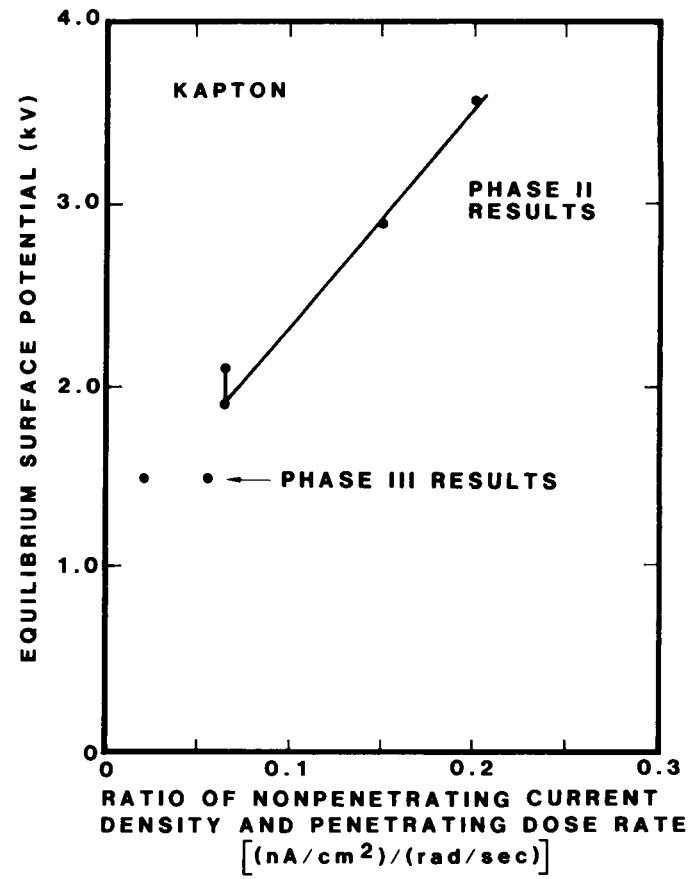

FIGURE 5. EQUILIBRIUM SURFACE POTENTIAL OF 2 mil KAPTON FOR VARIOUS COMBINED LOW AND HIGH ENERGY ELECTRON FLUX CONDITIONS

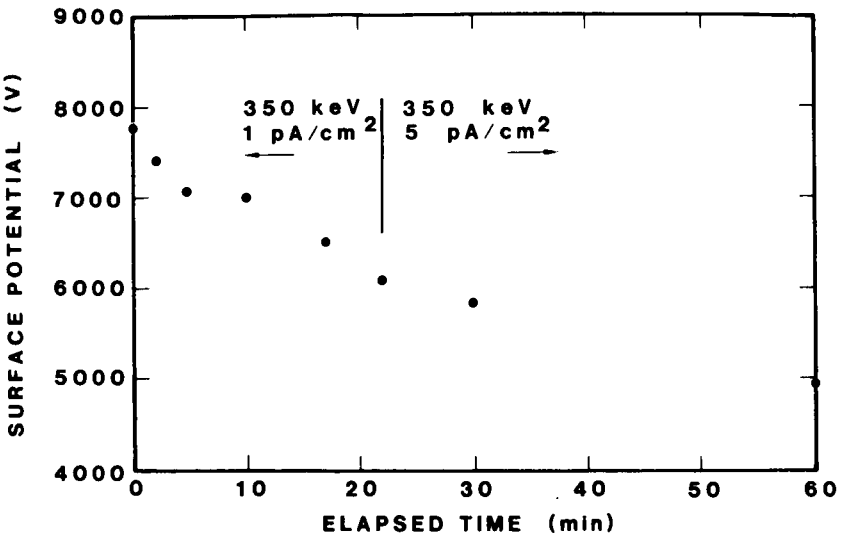

FIGURE 6. SSPM KAPTON SURFACE POTENTIAL VS TIME FOR HIGH-ENERGY ELECTRON EXPOSURE

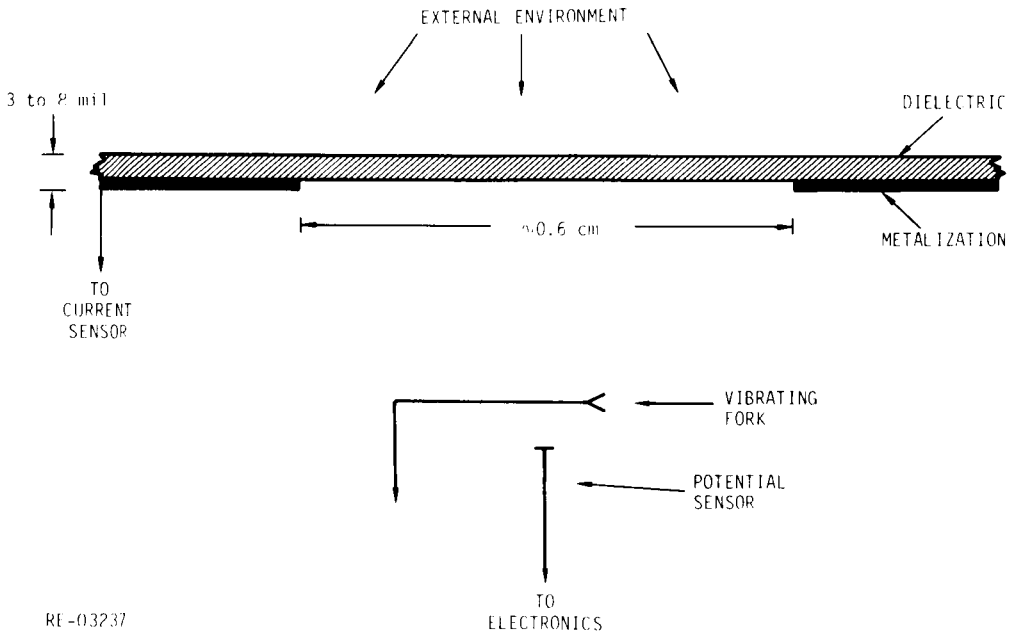

FIGURE 7. DIAGRAMATIC REPRESENTATION OF SSPM POTENTIAL AND CURRENT MONITORS